# Lab On a Chip System for Size-Based Gold and Polymer Nanoparticle Separation

**Jaeyun Yoon**
Nanyang Technological University
**Insup Kim**
Korea Advanced Institute of Science and Technology (KAIST)
**Suhan Lee**
Korea Advanced Institute of Science and Technology (KAIST)
**Wan-Sik Won**
Nanyang Technological University
**Jinhong Noh**
Korea Advanced Institute of Science and Technology (KAIST)
**Noori Kim**
Newcastle University in Singapore
**Yong-Jin Yoon** ( yongjiny@kaist.ac.kr )
Korea Advanced Institute of Science and Technology (KAIST)

**Research Article**

**Keywords:** Nanoparticle separation, Point-of-care (POC) application, Lab on a Chip (LOC) system, Ultrasonic irradiation, Acoustic agitation,

**Posted Date:** November 29th, 2021

**DOI:** https://doi.org/10.21203/rs.3.rs-1106285/v1

# Abstract

Despite the increasing demand for nanoscale biomolecule analysis for point-of-care (POC) application, nanoparticle separation remains a challenge in many applications due to huge sample loss during separation, low throughput, large scale input materials requirement, and sophisticated technologies. As the separation efficiency may affect the subsequent sample processing and analysis, a robust and reliable size-based separation technique is necessary. This study presents a lab on a chip system to enhance the separation performance by using rapid and straightforward polymer prototyping. In particular, the system consists of a microfluidic network with embedded membrane filters with different pore size cut-offs and an ultrasonic transmitter for acoustic agitation. Using the novel system, we successfully demonstrate the fractionation of 15 nm Au NP from polydisperse nanoparticle solution in the presence of ultrasonic wave (28-40 kHz) generated by the transducer incorporated with the microfluidic system during the separation. Ultrasonic irradiation helps in preventing cake formation and reversing the fouling process by acoustic agitation. The suggested system significantly increases the flow rate during the separation process and improves the recovery of target size nanoparticles. This microfluidic platform is expected to serve as a powerful tool for sample preparation and analytical methodology in POC applications.


# Introduction

With the growth in microfluidic technologies in the COVID-19 era, a substantial advance in the Lab-on-a-Chip (LOC) system has been presented, enabling miniaturization and integration of complex functions routinely performed by hand in the traditional analytical processes[1–3]. One of the most active applications in the LOC is observed in biomedical research with Point-of-care (POC) diagnostic devices. The POC diagnostic system can rapidly deliver diagnostic outcomes to patients providing the users with many benefits over the traditional diagnostic methods such as straightforward and easy-to-use interface, portability, less sample and reagent consumption, etc[4].

In biomedical research, size-based particle separation plays a significant role in the sample preparation process and the detection of target species[5,6]. As the size of analytes in biological research range from angstrom to millimetre scale, the separation mechanism of choice depends on their dimensions. During the past decade, many size-based separation techniques have been established for biomedical applications[5,7]. Enormous progress has been made, and size-based separation technologies move towards the miniaturized platforms to meet the requirements for point of care testing[8–10]. Many detection techniques require isolating target species of interest from solutions during sample preparation to provide unbiased and accurate insights into the biological process or phenomena. Since the dimension of biological structures ranges from angstrom to millimetre scale, the separation method varies depending on the target size due to the growing need for robust and reproducible size-based particle separation techniques. Especially, significant efforts have been put into developing a miniaturized size-selective particle sorting method for point of care applications such as LOC particle sorters[8–10]. However, the LOC

based separation techniques are limited to the sub-micron scale (such as cells, viruses, bacteria), which results in significant sample loss, diagnostics misinterpretation, and poor detection limit[11–14]. Developing robust and reliable size-based particle separation techniques is emerging as an essential prerequisite for nanoscale measurement to obtain insights into the various biological systems on a nanometer scale.

For nanoscale biomolecule sorting, biomedical research has carried out several size-dependent nanoparticle separation techniques such as technology-based on external fields application, physical sieving and size-selective precipitation. Unfortunately, commonly used current technologies for NP separation were still not sufficiently efficient in selectively sorting particles based on their size or molecular weight for proper POC use due to their complex hands-on processes and incompatibility with downstream analytical devices. A miniaturized, compact, cost-effective platform for size-based separation is more favourable than one in centralized laboratories to eliminate the need for bulky and sophisticated instruments and extensive input material and minimize the complexity of the device operation.

For nanoscale biomolecule separation, several size-dependent nanoparticle separation techniques have been employed. Based on the separation mechanism, these techniques fall into three categories: the use of external fields (centrifugal[15–17], electrical[18–20] and magnetic[21,22]), physical barriers for sieving[23], and size-dependent precipitation[24]. One of the most widely used methods based on the application of external fields is field flow fractionation (FFF). FFF is a particle separation technique taking advantage of the field exerted to a solution flowing through a channel. The field is perpendicular to the fluid flow, which results in the separation of particles suspended in the carrier solution due to the difference in travelling speed depending on their size and molecular weight. Despite its variations and versatility, it has not been widely used as a size based nanoparticle separation method due to its low throughput and extensive input material required. Alternatively, a size-dependent precipitation method has been devised. Size-dependent precipitation occurs when the stability, physical or chemical properties change depending on the surface chemistry of the nanoparticles. Sieving is another alternative for the size-selective fractionation of nanoparticles. Chromatography and membrane filtration employs physical barriers such as a column or physical hole to control elution and retention depending on the size of particles. Unfortunately, these traditional size based nanoparticle separation techniques result in huge sample loss, therefore, large input material is required. In addition, bulky instrumentation is involved in generating external field during the separation process. Due to the complexity of these technologies, there has been increasing demand for the development of miniaturized and compact platform for size-based separation, which can be used as a cost-effective preparative method in point of care application.

There have been many microfluidic approaches to bring the size-selective nanoparticle separation into miniaturized platforms. One of the most common separation mechanisms utilized in the microfluidic platform is membrane-based filtration because of its high resolution and straightforward procedure[25–28]. Gaborski *et al.*[23] demonstrated nanoparticle fractionation using porous nanocrystalline silicon membranes with resolution as high as 5 nm, potentially applicable to Lab-on-a-Chip system for dead-end

filtration. However, membrane filtration typically suffers from low efficiency associated with clogging and formation of cake layer near membrane filter[29], leading to low flow rate, sample loss, and high fluid resistance[30]. Also, the fabrication of nanopores involves a complicated and time-consuming micro-fabrication process due to nanoscale particle separation. To circumvent this limitation, "filter-free" microfluidic separation techniques have been developed. Microfluidic approaches based on electrophoresis, field-flow fractionation (FFF)[31,32] and centrifugation[15,17] have been devised and implemented for size-based nanoparticle separation and fractionation. However, these techniques still rely on external fields which usually need the bulky instrument to manipulate particle motion.

Furthermore, most passive separation techniques require expensive fabrication to build microstructures. For a point-of-care application, lab on a chip system that can be realized with a simple fabrication process, providing a user-friendly interface enabling easy sample handling, yet with high resolution with minor sample loss is necessary. For these reasons, the lack of reliable size-selective nanoparticle separation is a bottleneck in analyses of nanoscale biomolecules such as ribosome profiling, which requires size-selective separation of monosome from polysome molecules[33].

As membrane filtration can provide the most straightforward processing and high resolution, it has many advantages over filter-free alternatives. Hence it can be an excellent size-selective nanoparticle separation tool as long as the problems associated with membrane fouling during the process is addressed.As a part of its effort, many publications and research works have improved membrane filtration by utilizing ultrasonic treatment of membrane filters. However, most results focused on bulk processing for industrial use, such as wastewater processing, food processing, and ultrapure water production[34,35]. Typically, they employed ultrasonic bath, which requires high energy consumption and extensive input material, and it may not be suitable for biological applications where available input material is low.

To realize simple and rapid size-selective nanoparticle separation for POC application, we have developed a LOC system based on dead-end filtration by incorporating commercially available track-etched membrane filters with different pore sizes cut-off. Sample containing polydisperse nanoparticles has been processed in the microfluidic platform with embedded membrane filters. The dead-end filtration may cause clogging and membrane fouling due to the formation of a cake layer near the membrane surface, leading to low flow rate and membrane and sample loss damage. We have introduced ultrasonic treatment by integrating ultrasonic transmitters with a membrane filtration system online to overcome this issue. Ultrasonic assisted membrane filtration was modified to bring it into a miniaturized microfluidic platform. The functionality of this novel LOC based technology was confirmed by demonstrating size based gold and polymer nanoparticle separation.

## Materials And Methods

# 1. Basic principles of dead-end membrane filtration

Typically, the input fluid flow in dead-end membrane filtration is perpendicular to the membrane surface, called the "feed" solution. Driven by pressure in the filtration system along the channel, a fraction of the fluid passes through the membrane pores, called "filtrate" or sometimes "permeate". Moreover, a fraction of the input remains on the membrane surface, called "retentate". To quantify membrane-based filtration performance, permeates and retentates are collected separately and investigated by various analysis methods. When the targeted nanoparticle is a metal such as gold or silver, absorbance measurement is one way to quantify the performance. For small gold nanoparticles (~30 nm), the surface plasmon resonance effect induces the absorption maximum at 526 nm wavelength. For relatively large gold nanoparticles (60 nm), the absorption maximum is generated at 540 nm wavelength. Hence, the UV-Vis spectrometer is a valuable tool for identifying the size of the gold nanoparticles. Measuring the absorption from the collected filtrate and retentate samples can quantify the fraction of target size nanoparticles in each sample. From the absorption measurement data, the performance of the dead-end membrane filtration system can be determined.

# 2. Working principle of ultrasonic-assisted nanoparticle separation

The working principle of ultrasonic-assisted nanoparticle separation on a microfluidic device is illustrated in Fig. 1. The separation mechanism is straightforward using dead-end filtration. The microfluidic system for size-based nanoparticle separation consists of a microfluidic device with track-etched polycarbonate membrane filters with sharp pore size cut-off incorporated with an ultrasonic transducer. To isolate monodisperse nanoparticles from the mixture, membrane filters with a pore size larger and smaller than the particle size were used. As shown in Fig. 1, target (Green) particles penetrate the membrane with a greater cut-off value while larger particles settle onto the membrane. A membrane with a smaller cut-off was introduced to capture target particles enabling purification before collecting target particles. Impurities and particles smaller than the target flow through the second membrane filter and proceed to the waste reservoir.

One of the critical limitations in dead-end filtration is sample loss and decrease in permeability during the separation process due to particle adsorption on the membrane surface and the formation of a cake layer near the surface. An ultrasonic wave was exploited to detach fouled particles on the surface and enhance the target recovery of particles. (Fig. 2) The transducer was located near the membranes for efficient ultrasound irradiation to minimize the attenuation as the wave propagates through the material. And the chamber was designed to fit the active area of the transducer to maximize the coverage of ultrasound irradiation. Negative pressure was applied through the outlet to prevent leakage at the interface of the PDMS layer and the membranes.

# 3. Chip design and fabrication

The microfluidic nanoparticle separation device prototype was designed using AutoCAD software and constructed by a standard soft lithography process. The device consists of two circular reservoirs

connected by a microfluidic network to filtrate nanoparticles, as illustrated in Fig. 3. The microfluidic network patterned onto the bottom layer, which connects the two reservoirs. The side channels connected to the reservoir for sample collection are patterned onto the middle layer. And the top layer serves as a top cover to form a closed microfluidic network while the left reservoir remains open for sample loading. The right reservoir has microfluidic barrier structures to guide the fluid flow uniformly to cover the entire surface of the membrane, and it enables the even distribution of the particles to infiltrate the membrane surface.

The left reservoir serves as a sample loading well where a mixture of nanoparticles was loaded. The membrane filters with different pore sizes, including 15 nm and 30 nm, were integrated with three PDMS layers in the 20 nm NP separation process. First, the structures of each PDMS layer were patterned onto a transparency mask and supplied by Fineline Imaging (Colorado Springs, CO) at 32000 dpi resolution. To fabricate a master mould, SU-8 2025 was spun onto a silicon substrate using a spin coater at 2000 rpm for 30 sec to achieve a uniform thickness of 40 um. Then the master went through a soft bake process to evaporate solvent at 65 °C for 2 min and 95°C for 5 min followed by UV exposure (200 $mJ/cm^2$) for 30 sec. For Post-exposure bake (PEB), the master was cured at 65 min for 1 min and 95 min 3 min. Then the pattern was developed by immersing the master in the developer solution for 5 min and rinsing with Deionized water and isopropyl alcohol.

Excess water must be removed in a spin dryer. After the patterning process, the SU-8 mould was modified with trimethylchlorosilane (Sigma-Aldrich, USA) under vacuum. Next, the PDMS layers were fabricated by standard soft lithographic techniques. Briefly, PDMS was mixed with a curing agent at a ratio of 10:1, and it poured onto the SU-8 master mould to form a replica of the device. Degassing was performed to remove entrapped bubbles from the layer. Then the layer was baked in a convection oven at 65 °C for an hour for curing and peeled off from the master mould. Two reservoir regions were punched with biopsy punches, and holes at the inlet and outlet were punched for fluidic access.

Membrane filters were cut using the laser cutting process into the desired size. Pore sizes of membrane filters varied depending on the target nanoparticle size. Uncured elastomer/curing agent mixture was applied along the reservoir's edge to integrate the membrane filter on the PDMS bottom layer. Then the membrane was aligned, placed at the centre of the reservoir, and pressed gently with a round tip tweezer to absorb the uncured mixture into the filter layer. The bottom layer and membrane filter were cured in an oven at 65 °C for at least 30 min. Three PDMS layers were oxygen plasma treated to activate the surface, aligned and brought into contact with each other to form a microfluidic platform. Tygon tubings were inserted into through holes at inlets and outlet regions. After integration and assembly, no significant leak was observed during operation. SU-8 master mould can be reused after washing with IPA and deionized water. The microfluidic device was coupled with ultrasonic transducers by using silicone at the interface of the transducer and PDMS layer to minimize the energy loss and attenuation during operation.

# 4. Ultrasonic assisted nanoparticle separation on a microfluidic device

Before separation, the microfluidic network was rinsed with 0.1% Poly(ethylene glycol)-*block*-poly(propylene glycol)-*block*-poly(ethylene glycol) (Pluronic F108)(Sigma-Aldrich) solution to remove residual impurities and treat the fluidic PDMS surface, thereby preventing adsorption of nanoparticle on the membrane surface or fluidic channel wall and formation of fouling on the membrane surface. Gold nanoparticles (Nanocs, NY, USA) with a varied diameter (15, 30, 50, 80, 100, 200, 400, 600 nm) were used to demonstrate ultrasonic-assisted nanoparticle separation on microfluidic devices. In the case of 60 nm/ 100 nm mixture, 10 µl of the stock solution of 60 and 100 nm ($1.9 \times 10^9$ / mL and $3.8 \times 10^9$ / mL respectively) Au nanoparticles in 0.1mM PBS were added into 1 × PBS, and the final volume was brought up to 100 µl. The mixture was loaded into a sample reservoir of an assembled microfluidic device with a membrane filter for separation. (Fig. 4) The mixture was driven into the microfluidic device by the negative pressure generated by the syringe pump operating on "withdraw" mode. Flow velocity was set to 0.1 mL/h. The microfluidic device was irradiated with ultrasonic waves generated by the ultrasonic transducer during the separation. Typically, a 40 kHz square wave was developed by a function generator and 50 times amplified through a high voltage amplifier (WMA-300, Falco systems) and used to excite the ultrasonic transducer. During the separation process, other inlets and outlets were closed than the waste port. Before collecting target particles, 0.1 % luronic F108 solution was injected at 0.1 mL/h for 10 min as a washing buffer. Backwashing with the ultrasonic wave was performed to retrieve 60 nm gold nanoparticle (target) from the chamber region between two membrane filters. 60 nm gold nanoparticles (Au NP) were collected in either 0.1 % 108 solution or PBS for downstream analysis. The retentate settled on the first membrane was collected by pipetting up and down several times for measurement.

# 5. Characterization of Populations of Nanoparticles

UV-Vis spectroscopy was used to characterize the populations of nanoparticles before and after the filtration process by quantifying the absorption intensity of each solution. Populations of nanoparticles were characterized by measuring peak absorbance and intensity wavelengths on a multimode plate reader (Perkin Elmer). The wavelengths of peak absorbance depend on the sizes of gold nanoparticles. Typically, peak absorbance occurs within 564 – 574 nm and 538 – 544 nm for 100 nm and 60 nm Au NP. Samples (Filtrates, retentates) collected from the microfluidic device after separation were analyzed within the 400 – 700 nm wavelength range, and the results were compared with that of the stock solution. Based on concentration and volume loaded, the recovery rate and sample loss were calculated.

To validate the filtration efficiency fluorescence image was obtained using a fluorescent microscope. 350 and 450 nm fluorescently labelled polystyrene nanoparticles were filtered on a microfluidic device incorporated with a 400 nm pore membrane filter to visualize NP adsorbed onto the membrane surface. The membrane was taken out of the device and investigated under a microscope. The 450 nm particles settled onto the membrane were considered sample loss, and the number of particles was counted automatically using Image J software.

In addition, particle size distribution was also determined by dynamic light scattering (DLS) using isolated filtrate and retentate prepared in 0.1% F108 solution. The distribution data were acquired and

compared with the distribution data of each stock solution. All experiments were carried out at least 3 times.

## Results & Discussion

# 1. Characterization of microfluidic size based NP separation with ultrasonic irradiation

The efficiency of nanoparticle filtration using the microfluidic system with ultrasonic irradiation was evaluated using monodisperse 60 nm gold nanoparticles and a single track-etched polycarbonate membrane filter with 80 nm pore size cut-off. (Fig. 5) Twenty microliters of gold nanoparticle stock solution were diluted with 80 μL 0.1% F108 solution and placed into a loading reservoir. Filtration was performed with ultrasonic irradiation to investigate the efficiency of ultrasonic treatment, and the UV-Vis spectroscopy results were compared with the results of filtration without irradiation. To obtain a monodisperse target size, maximizing the recovery rate while no detectable particles from the retentate solution are essential. Recovery rates and loss were calculated through normalization by the absorbance profile of the feed solution. Significant sample loss was observed after the filtration when ultrasonic irradiation was not performed. It is likely due to the adsorption of particles onto the membrane surface during the process. Peak absorbance of filtrate indicates that 21% of input was recovered after filtration, yielding a prolonged recovery rate. From the peak absorbance of retentate, we assumed 17.9% of input could not penetrate the membrane, and the particles were retrieved by manual pipetting. On the other hand, with ultrasonic irradiation, a significant enhancement in recovery rate was observed. The absorbance of the retentate solution was negligible, indicating few 60 nm particles were recovered in the solution. It achieved a 70.6% recovery rate introducing ultrasonic treatment during the separation on a microfluidic device, which is 3.9 times higher than without ultrasonic treatment.

# 2. Effect of surface treatment

In the initial attempt to determine the filtration efficiency of the microfluidic device, it was found that the filtration efficiency is greatly dependent on the membrane surface condition. Once the volume loaded into the sample reservoir passed through the membrane, and the membrane surface started to dry, Au NP settled on the membrane surface were compacted. And the foulants formed a cake layer, making it challenging to re-suspend particles from the membrane surface for downstream analysis regardless of vigorous pipetting. The membrane filter surface must be kept wet during and after the filtration to maximize efficiency and recovery. Monodisperse fluorescently labelled polystyrene (PS) NPs demonstrated this phenomenon, visualizing it using a fluorescent microscope. The hydraulic diameter of NP was 450 nm, and the pore size cut-off of the membrane filter used for filtration was 400 nm. Fig. 6

shows the comparison of removal rate between the cases with and without ultrasonic treatment, either on wet or dry surfaces. Fig. 6-1 showed the 450 nm particles on the 400 nm filter surface when 100 μl of sample passed through the membrane. Under wet surface conditions (Fig. 6-2 and 3), the effectiveness of ultrasonic cleaning was examined. As a result, most input particles were successfully removed from the

filter surface by both backflushing or pipetting. After filtration without ultrasonic treatment, the loss was 5%, while no detectable quantities of nanoparticles were found from the surface after ultrasonic cleaning. This result indicates that nanoparticles largerthan the pore size of the membrane filter tend to stay in suspension under the wet surface condition. The cake layer formed during the filtration is easier to remove from the membrane surface during the cleaning process combined with ultrasonic irradiation. In contrast to a wet surface, severe fouling of membrane filter was observed once the membrane surface was dry, indicating the irreversible formation of cake layer with foulants on the surface under dry surface conditions. (Fig. 6-4 and 5) Ultrasonic irradiation exhibited an improvement in removal rate. However, significant losses were detected from both cases. As a result, 65% of input particles were successfully removed from the surface without ultrasonic cleaning, while 70% of input were removed by ultrasonic cleaning. Hence, we assumed that 30% of nanoparticles larger than pore size were presumably adsorbed on membrane surface irreversibly under dry surface conditions. Therefore, the membrane filter surface needs to remain wet during and after filtration before recovering target particles, and ultrasonic cleaning enhances the removal of particles from the surface.

To examine the utility of the microfluidic device in size based nanoparticle sorting, filtration of 100 / 400 nm NP mixture was performed, and the particle size distribution was investigated by dynamic light scattering (DLS) technique. (Fig. 7) A mix of two different sized polystyrene particles was driven into the microfluidic device and pressurized to initiate size based filtration. For 100 / 400 nm separation, 80 nm and 200 nm track-etched membrane filter was selected for separation. The filtrate was collected from the reservoir by backflushing with ultrasonic treatment. Fig. 7 shows particle size distribution profiles of 100 nm and 400 nm particle stock solution, filtrate and mixture. Size distribution of the polydisperse mixture was examined before filtration. As a result, the filtrate showed a size distribution profile similar to the original 100 nm stock solution without a detectable shift in peak wavelength and spectrum broadening. We compared the size distribution profile measured by the light scattering technique to the size estimated by absorbance spectra. As a result, peak absorbance of the filtrate was ~70% of stock solution with slight variation in peak wavelength, indicating successful size discrimination and a high recovery rate.

# 3. Effect of orientation of the ultrasonic treatment

The effect of orientation of ultrasonic transmitter on the performance of the device in particle fractionation and recovery rate was investigated using 60 nm Au NP. Particle fractionation was carried out with track-etched membrane filters, with the mean pore sizes cut-off of 80 nm. The ultrasonic transmitter was incorporated into the device at the feed side or permeate side to examine the effect of the orientation of the ultrasonic transmitter on the fractionation capability. The 40 kHz square US waves were irradiated on the membrane from the permeate side or feed side. Fig. 8A shows the layouts of the microfluidic particle filtration system with the embedded ultrasonic transmitter. Output voltage through amplifier was 40 Vp-p. The 50 µl of 60 nm particle stock solution was diluted with 50 µl 0.1% F108 surfactant solution to investigate ultrasonic-assisted filtration performance. To initiate filtration, 100 µl of the sample was driven into the device. 100 µl of 0.1% F108 was reloaded when the first sample passed so that the residual particles were collected in the collection reservoir to maximize the recovery. After the

filtration, collected samples were examined using a UV-Vis spectrophotometer, and an absorbance spectra scan was performed within the 350 - 700 nm wavelength range. As a result, the higher recovery rate of 60 nm Au NP was obtained from the sample filtered using feed side ultrasonic treatment at the input concentration studied. (57%) (Fig. 8B) In the case of ultrasound irradiation at the permeate side of the membrane, it yielded 48% of the original concentration using the same input sample.

In addition, the volumetric flow rate was monitored every 30 sec up to 20 min using each transmitter configuration under the same pressure and input concentration condition. (Fig.9) As a result, a similar trend was also seen in volumetric flow rate results. The higher volumetric flow rate was achieved when ultrasound was irradiated onto the membrane surface from the feed side of the membrane. A significant decrease in flow rate occurred after 5 min filtration when ultrasound was irradiated from the permeate side of the membrane, indicating critical fouling of the membrane. Despite the decrease in flow rate in ultrasound irradiation from the feed side, the flow rate was stabilized after 10 min initial separation process. On the other hand, flow rate consistently decreased in ultrasonic irradiation from the permeate side, showing a similar trend as with no ultrasonic treatment. The flow rate was double with ultrasonic irradiation compared to no ultrasonic treatment when the ultrasonic propagated from the feed side. According to the flow rate results, we assumed that the orientation of the ultrasonic transmitter affected the effectiveness of the ultrasonic treatment in preventing the formation of cake layer and fouling of membrane as well as recovery of the target particle

# Conclusions

The LOC system for size-based NP separation using dead-end membrane filtration has shown a significant improvement in separation performance employing ultrasonic agitation. Even though many studies have been reported for ultrasonic-assisted filtration, most of them were practised in macroscale with sophisticated ultrasonic transducer system. The LOC system suggested here uses rapid and straightforward integration of ultrasonic transducer into the microfluidic system and enables nanoscale particles.

Using the novel method, we have fractionated 15 nm Au NP from polydisperse (15/30 nm) nanoparticle solution in the presence of ultrasonic wave (28-40 kHz) transmitted by the transducer integrated with the microfluidic system during the separation. The suggested technique has prevented the cake layer formation and foulant adhesion to the membrane surface by agitation. Typically, the processing time has been ~10 min by enhancing the flow rate in the presence of ultrasonic treatment during the process. In addition, it has achieved 70% of the recovery rate in Au NP separation, showing significant improvement in recovery rate compared to the case without ultrasonic treatment. The novel microfluidic lab on a chip has held great potential as a helpful tool that provides many advantages over other microfluidic size-based techniques such as 1) simple fabrication by employing commercially available track-etched membrane filter with sharp pore size cut-off to bypass complicated fabrication process for building sieving microstructure, 2) easy sample handling utilizing automatic process, 3) high recovery rate (70% in case of 60 nm Au NP) of target size NP, 4) No additional chemical pretreatment required by using

membrane filtration 5) Fast and straightforward processing, 6) Little dilution of the sample. This LOC approach is the first nanoparticle separation method based on a combination of dead-end membrane filtration and ultrasonic treatment in a microscale environment to the best of our knowledge.

As these techniques are still at an early stage of development, they need system-level verification of feasibility for real-world application. The next step to further investigate the feasibility of this LOC system is to exercise size-selective separation using biosample. Monosome(~30nm) separation will be carried out using the LOC system as a preparative sample processing in ribosome profiling to show the system's feasibility for both research and clinical use.

# Declarations

This work was supported by the Korea Institute of Energy Technology Evaluation and Planning (KETEP) and the Ministry of Trade, Industry & Energy (MOTIE) of the Republic of Korea (No. 20194030202360) and the MSIT(Ministry of Science, ICT), Korea, under the High-Potential Individuals Global Training Program)(2020-0-01580) supervised by the IITP(Institute for Information & Communications

### Author Contributions

J.Y. and I.K. conceived the study and performed the experiments, analyzed the data, and wrote the original draft. S.L., W.-S.W., and J.N analyzed the data and provided comments on methods. N.K. interpreted the data and reviewed the manuscript and provided inspiring suggestions for improvement. Y.-J.Y. conceived and supervised the project. J.Y and I.K. are co-first authors. Y.-J.Y. is the primary corresponding author and N.K. is also a co-corresponding author. All authors contributed to writing the manuscript.

### Competing Interests Statement

The authors declare no competing interests.

# References

1. Chan, W. X., Kim, N., Ng, S. H. & Yoon, Y. J. Acoustic energy distribution in microfluidics chip via a secondary channel. *Sensors and Actuators B: Chemical*, **252**, 359–366 https://doi.org/doi:10.1016/j.snb.2017.05.166 (2017).
2. Kim, N., Chan, W. X., Ng, S. H. & Yoon, Y. J. An acoustic micromixer using low-powered voice coil actuation. *Journal of Microelectromechanical Systems*, **27**, 171–178 https://doi.org/doi:10.1109/JMEMS.2017.2788566 (2018).
3. Kim, N., Chan, W. X., Ng, S. H., Yoon, Y. J. & Allen, J. B. Understanding interdependencies between mechanical velocity and electrical voltage in electromagnetic micromixers. *Micromachines*, **11**, 636 https://doi.org/doi:10.3390/mi11070636 (2020).

4. Kim, N., Han, K., Su, P. C., Kim, I. & Yoon, Y. J. A rotationally focused flow (RFF) microfluidic biosensor by density difference for early-stage detectable diagnosis. *Sci. Rep*, **11**, 1–12 https://doi.org/doi:10.1038/s41598-021-88647-0 (2021).
5. Wu, M. *et al.* Acoustic separation of nanoparticles in continuous flow. *Advanced functional materials*, **27**, 1606039 https://doi.org/doi:10.1002/adfm.201606039 (2017).
6. Robertson, J. D. *et al.* Purification of nanoparticles by size and shape. *Scientific reports*, **6**, 1–9 https://doi.org/doi:10.1038/srep27494 (2016).
7. Kowalczyk, B., Lagzi, I., Grzybowski, B. A. & Nanoseparations Strategies for size and/or shape-selective purification of nanoparticles. *Current Opinion in Colloid & Interface Science*, **16**, 135–148 https://doi.org/doi:10.1016/j.cocis.2011.01.004 (2011).
8. Balyan, P., Saini, D., Das, S., Kumar, D. & Agarwal, A. Flow induced particle separation and collection through linear array pillar microfluidics device., **14**, 024103 https://doi.org/doi:10.1063/1.5143656 (2020).
9. Lenshof, A. & Laurell, T. Continuous separation of cells and particles in microfluidic systems. *Chem. Soc. Rev*, **39**, 1203–1217 https://doi.org/doi:10.1039/B915999C (2010).
10. Sajeesh, P. & Sen, A. K. Particle separation and sorting in microfluidic devices: a review. *Microfluidics and nanofluidics*, **17**, 1–52 https://doi.org/doi:10.1007/s10404-013-1291-9 (2014).
11. Dalili, A., Montazerian, H., Sakthivel, K., Tasnim, N. & Hoorfar, M. Dielectrophoretic manipulation of particles on a microfluidics platform with planar tilted electrodes. *Sensors and Actuators B: Chemical*, **329**, 129204 https://doi.org/doi:10.1016/j.snb.2020.129204 (2021).
12. Huh, D. *et al.* Gravity-driven microfluidic particle sorting device with hydrodynamic separation amplification. *Analytical chemistry*, **79**, 1369–1376 https://doi.org/doi:10.1021/ac061542n (2007).
13. Kuntaegowdanahalli, S. S., Bhagat, A. A. S., Kumar, G. & Papautsky, I. Inertial microfluidics for continuous particle separation in spiral microchannels. *Lab on a Chip*, **9**, 2973–2980 https://doi.org/doi:10.1039/B908271A (2009).
14. Shi, J., Huang, H., Stratton, Z., Huang, Y. & Huang, T. J. Continuous particle separation in a microfluidic channel via standing surface acoustic waves (SSAW). *Lab on a Chip*, **9**, 3354–3359 https://doi.org/doi:10.1039/B915113C (2009).
15. Yeo, J. C. *et al.* Label-free extraction of extracellular vesicles using centrifugal microfluidics., **12**, 024103 https://doi.org/doi:10.1063/1.5019983 (2018).
16. Akbulut, O. *et al.* Separation of nanoparticles in aqueous multiphase systems through centrifugation. *Nano letters*, **12**, 4060–4064 https://doi.org/doi:10.1021/nl301452x (2012).
17. Arosio, P., Müller, T., Mahadevan, L. & Knowles, T. P. Density-gradient-free microfluidic centrifugation for analytical and preparative separation of nanoparticles. *Nano letters*, **14**, 2365–2371 https://doi.org/doi:10.1021/nl404771g (2014).
18. Zhao, S. *et al.* A disposable acoustofluidic chip for nano/microparticle separation using unidirectional acoustic transducers. *Lab on a Chip*, **20**, 1298–1308 https://doi.org/doi:10.1039/D0LC00106F (2020).

19. Arnaud, I., Abid, J. P., Roussel, C. & Girault, H. H. Size-selective separation of gold nanoparticles using isoelectric focusing electrophoresis (IEF). *Chem. Commun*, 787–788 https://doi.org/doi:10.1039/B413719A (2005).
20. Hanauer, M., Pierrat, S., Zins, I., Lotz, A. & Sönnichsen, C. Separation of nanoparticles by gel electrophoresis according to size and shape. *Nano letters*, **7**, 2881–2885 https://doi.org/doi:10.1021/nl071615y (2007).
21. Shamloo, A. & Parast, F. Y. Simulation of blood particle separation in a trapezoidal microfluidic device by acoustic force. *IEEE Transactions on Electron Devices*, **66**, 1495–1503 https://doi.org/doi:10.1109/TED.2018.2889912 (2019).
22. Latham, A. H., Freitas, R. S., Schiffer, P. & Williams, M. E. Capillary magnetic field flow fractionation and analysis of magnetic nanoparticles. *Analytical chemistry*, **77**, 5055–5062 https://doi.org/doi:10.1021/ac050611f (2005).
23. Gaborski, T. R. *et al.* High-performance separation of nanoparticles with ultrathin porous nanocrystalline silicon membranes. *ACS nano*, **4**, 6973–6981 https://doi.org/doi:10.1021/nn102064c (2010).
24. Zhao, W., Lin, L. & Hsing, I. M. Nucleotide-mediated size fractionation of gold nanoparticles in aqueous solutions., **26**, 7405–7409 https://doi.org/doi:10.1021/la9044489 (2010).
25. Fan, J. B. *et al.* Bioinspired microfluidic device by integrating a porous membrane and heterostructured nanoporous particles for biomolecule cleaning. *ACS nano*, **13**, 8374–8381 https://doi.org/doi:10.1021/acsnano.9b03918 (2019).
26. De Jong, J., Lammertink, R. G. & Wessling, M. Membranes and microfluidics: a review. *Lab on a Chip*, **6**, 1125–1139 https://doi.org/doi:10.1039/B603275C (2006).
27. Noblitt, S. D. *et al.* Integrated membrane filters for minimizing hydrodynamic flow and filtering in microfluidic devices. *Analytical chemistry*, **79**, 6249–6254 https://doi.org/doi:10.1021/ac070943f (2007).
28. Wei, H. *et al.* Particle sorting using a porous membrane in a microfluidic device. *Lab on a chip*, **11**, 238–245 https://doi.org/doi:10.1039/C0LC00121J (2011).
29. Linkhorst, J., Beckmann, T., Go, D., Kuehne, A. J. & Wessling, M. Microfluidic colloid filtration. *Scientific reports*, **6**, 1–8 https://doi.org/doi:10.1038/srep22376 (2016).
30. Belfort, G., Davis, R. H. & Zydney, A. L. The behavior of suspensions and macromolecular solutions in crossflow microfiltration. *Journal of membrane science*, **96**, 1–58 https://doi.org/doi:10.1016/0376-7388(94)00119-7 (1994).
31. Shin, K. *et al.* Feasibility study for combination of field-flow fractionation (FFF)-based separation of size-coded particle probes with amplified surface enhanced Raman scattering (SERS) tagging for simultaneous detection of multiple miRNAs. *Journal of Chromatography A*, **1556**, 97–102 https://doi.org/doi:10.1016/j.chroma.2018.04.057 (2018).
32. Shendruk, T. N. *et al.* Field-flow fractionation and hydrodynamic chromatography on a microfluidic chip. *Analytical chemistry*, **85**, 5981–5988 https://doi.org/doi:10.1021/ac400802g (2013).

33. Ingolia, N. T., Brar, G. A., Rouskin, S., McGeachy, A. M. & Weissman, J. S. The ribosome profiling strategy for monitoring translation in vivo by deep sequencing of ribosome-protected mRNA fragments. *Nature protocols*, **7**, 1534–1550 https://doi.org/doi:10.1038/nprot.2012.086 (2012).
34. Kyllönen, H., Pirkonen, P. & Nyström, M. Membrane filtration enhanced by ultrasound: a review., **181**, 319–335 https://doi.org/doi:10.1016/j.desal.2005.06.003 (2005).
35. Shi, X., Tal, G., Hankins, N. P. & Gitis, V. Fouling and cleaning of ultrafiltration membranes: A review. *Journal of Water Process Engineering*, **1**, 121–138 https://doi.org/doi:10.1016/j.jwpe.2014.04.003 (2014).

# Figures

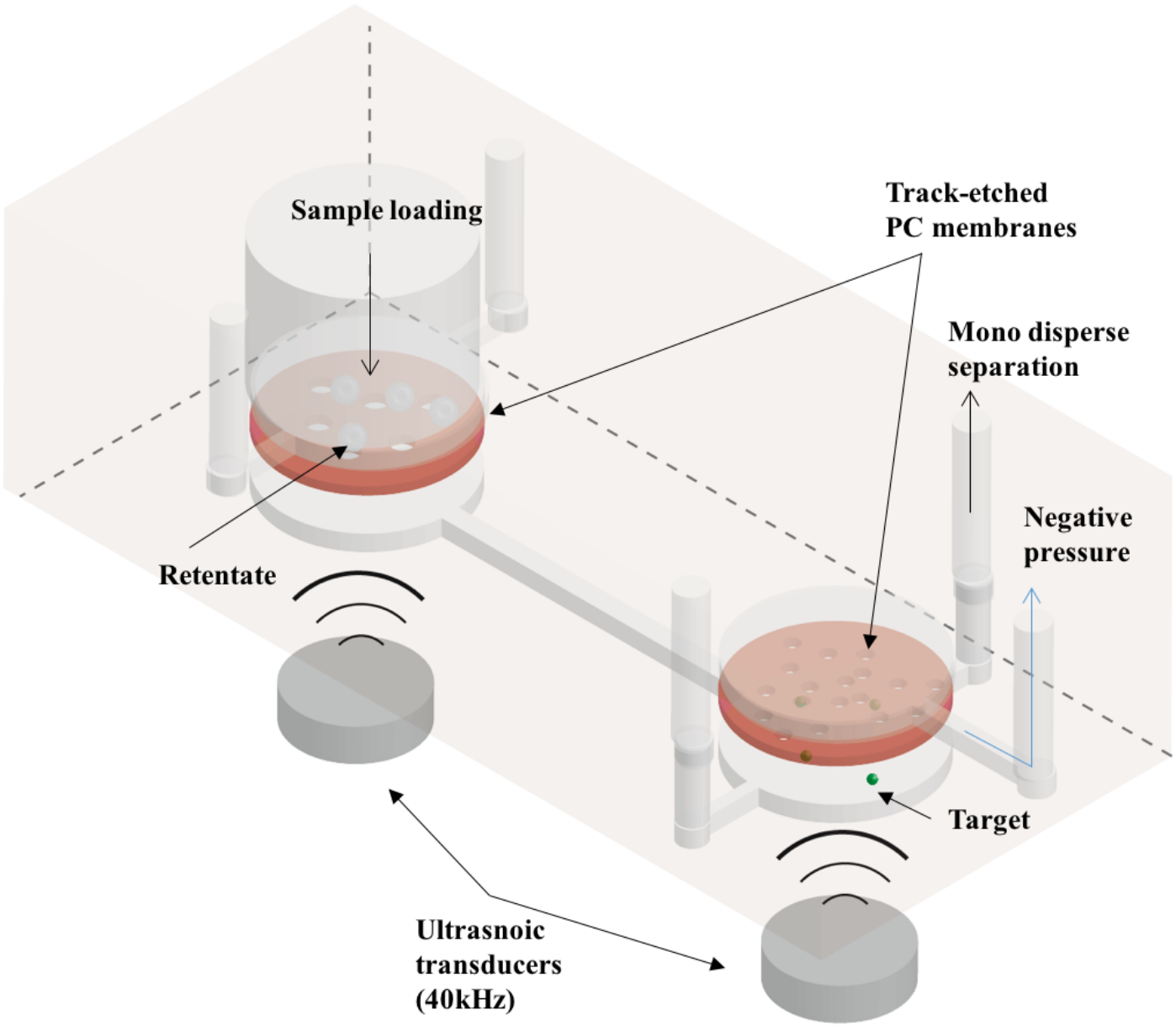


Figure 1

Schematic of a microfluidic platform for nanoparticle separation. Track-etched polycarbonate membranes with different pore sizes were embedded to capture target molecules. Particles more extensive than the cut-off of the first membrane will remain on the membrane (waste). In contrast, target molecules penetrate the first molecule with large pores and capture in a microchamber underneath the second membrane with the lower cut-off. Captured molecules are collected in an elution buffer by applying negative pressure to microfluidic networks connected to a syringe pump. Ultrasonic transducers were incorporated with the microfluidic platform to enhance recovery by detaching particles on the fouled membrane surface.

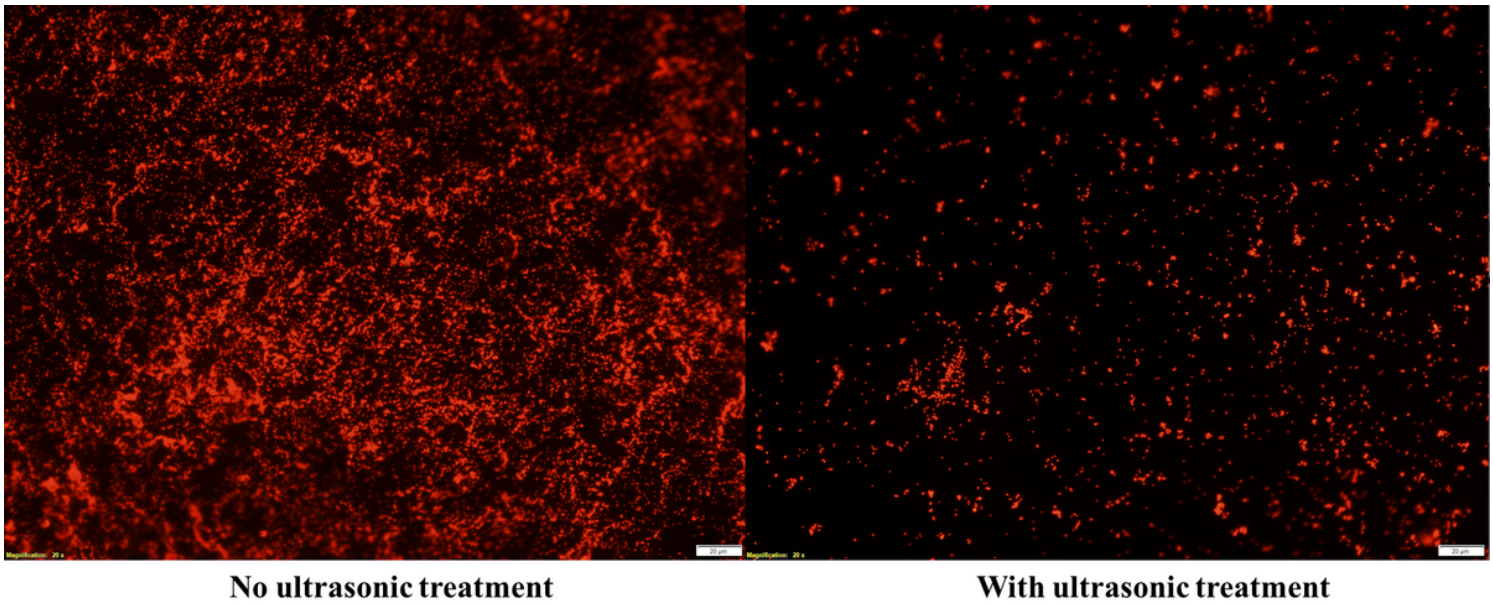


## Figure 2

Effect of ultrasonic treatment during NP separation

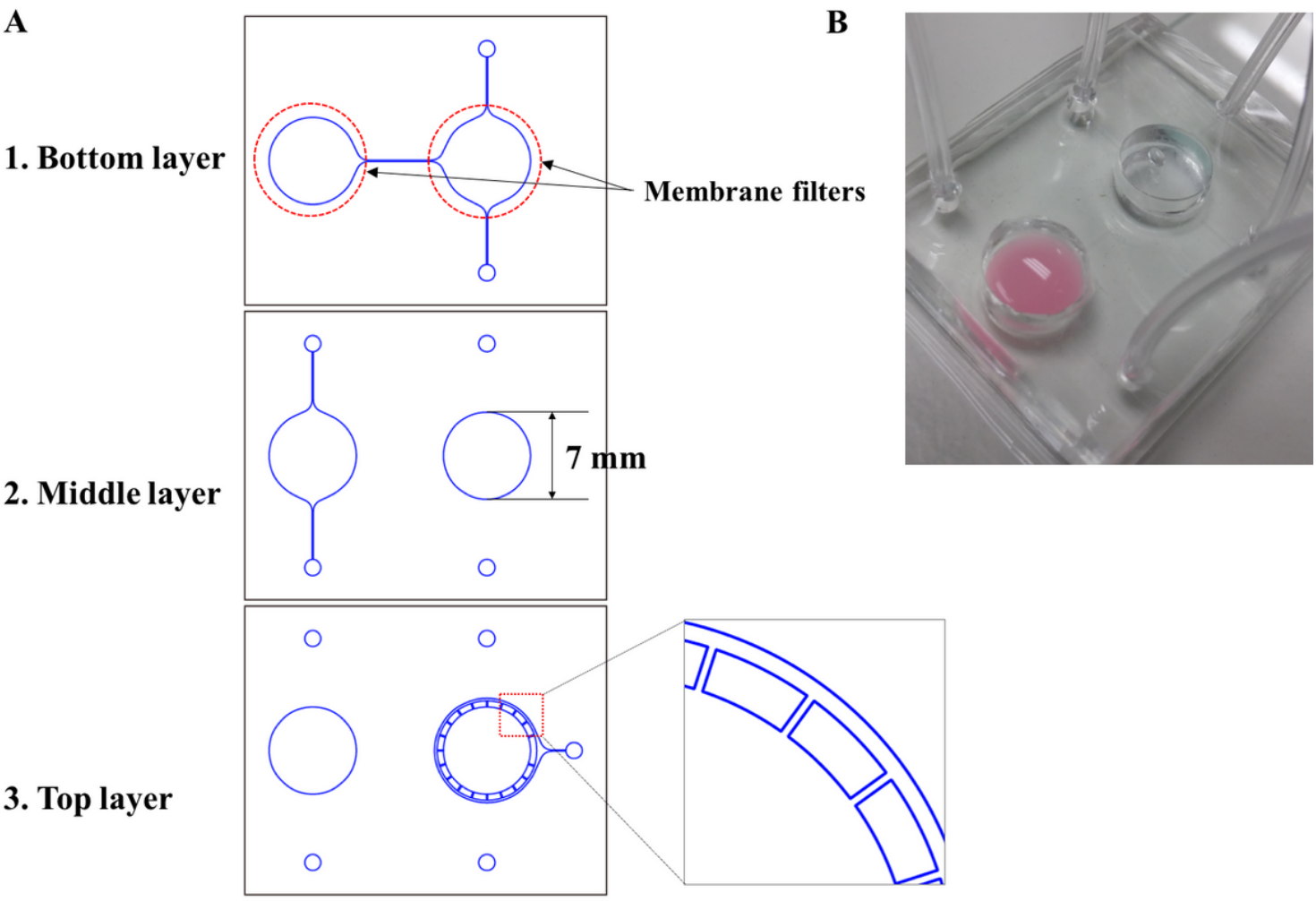


## Figure 3

Fabrication of microfluidic nanoparticle separation device. (A) Each PDMS layer was patterned by standard soft lithographic technique. Using an uncured PDMS prepolymer, membrane filters were embedded in the interface between the bottom and middle layers. The left reservoir served as a sample loading well. (B) A microfluidic nanoparticle separation device with a sample loaded in a sample reservoir.

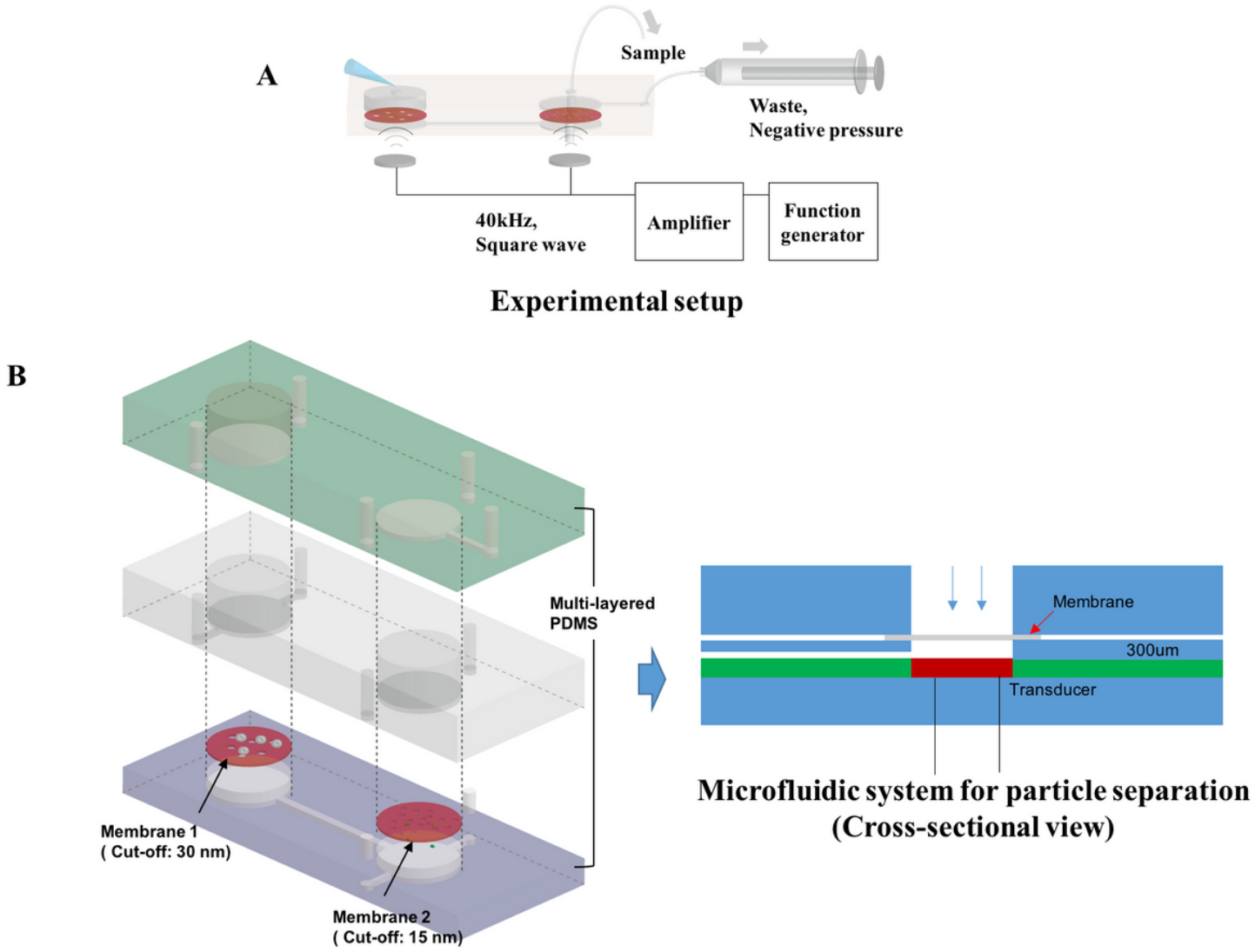


## Figure 4

Microfluidic device for on-chip nanoparticle separation consists of three PDMS layers. Membrane filters with different cut-off sizes (15 nm, 30 nm) were sandwiched between the bottom and middle layers in the case of 20/ 50 nm nanoparticle separation. Particles larger than the cut-off of the first membrane remain in the sample loading reservoir, and the rest can penetrate the membrane. Particles and buffer solution can go through the second membrane with a smaller cut-off (15nm), while the target size particle (20nm) stay in the chamber region between those two membrane filters.

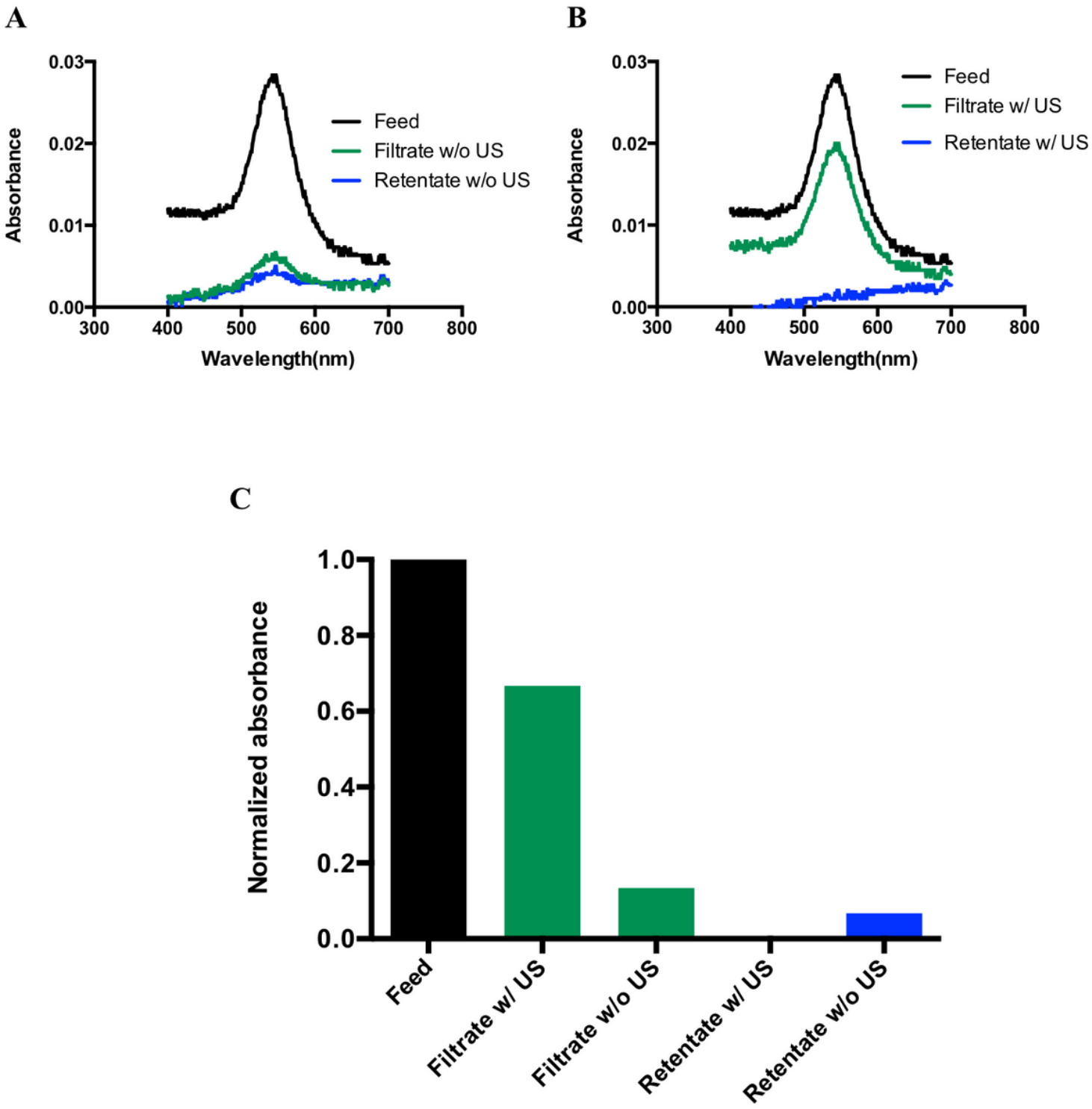


## Figure 5

60 nm Au NP filtration using membrane filter with 80 nm pore size cut-off embedded in the microfluidic size-based particle separation device. (A) The absorbance was measured using the feed, filtrate, retentate sample collected after filtration without ultrasonic irradiation. (w/o US) (B)The absorbance results were compared to the case with ultrasonic irradiation (w/ US). (C) In the presence of ultrasonic irradiation, 70.6 % of input 60 nm particles were successfully collected, while 21% of input particles were collected without ultrasonic treatment.

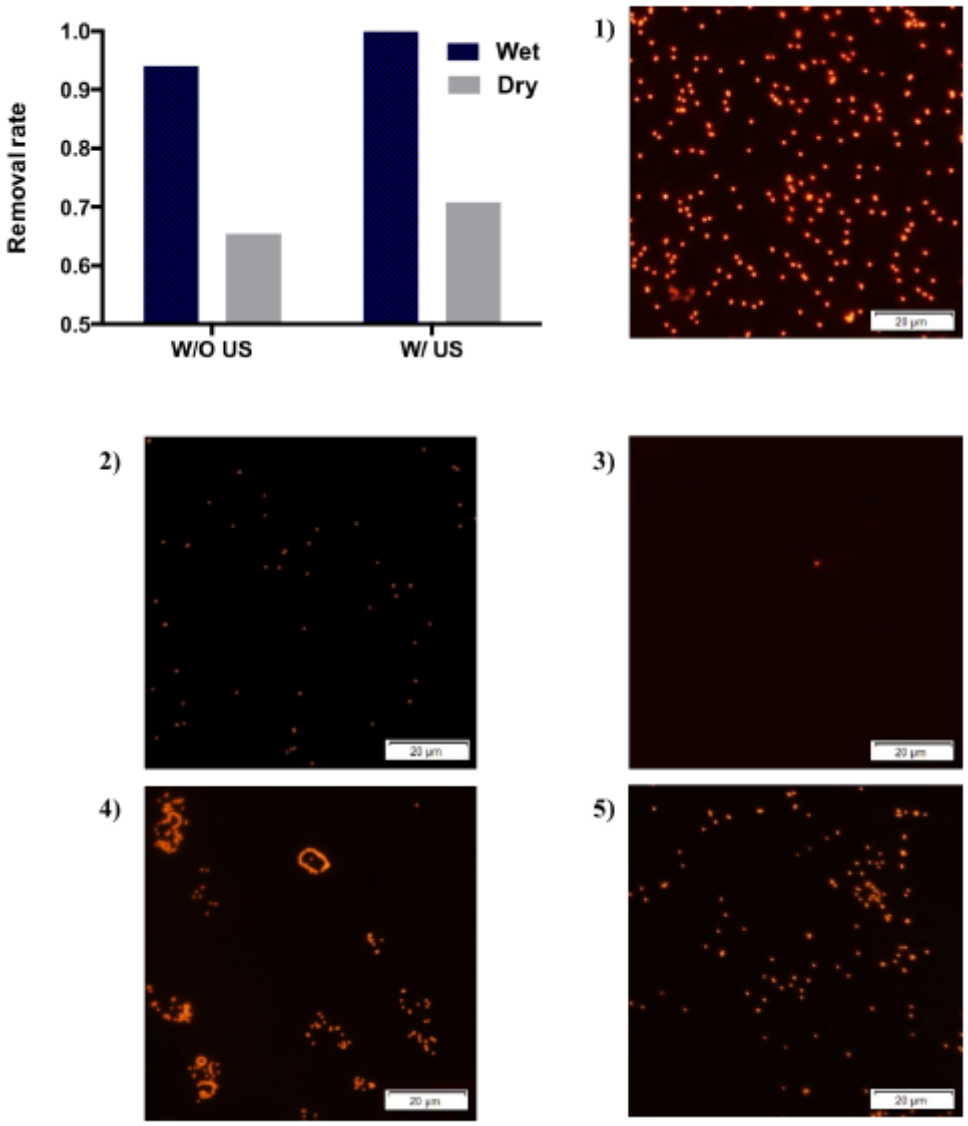


## Figure 6

Comparison of particle removal rate under different surface conditions (wet/dry). Under the dry surface condition, particles irreversibly formed the cake layer near the membrane filter surface, yielding a 65 -70 % recovery rate. On the other hand, most input particles are collected when the membrane filter remains wet during the filtration.

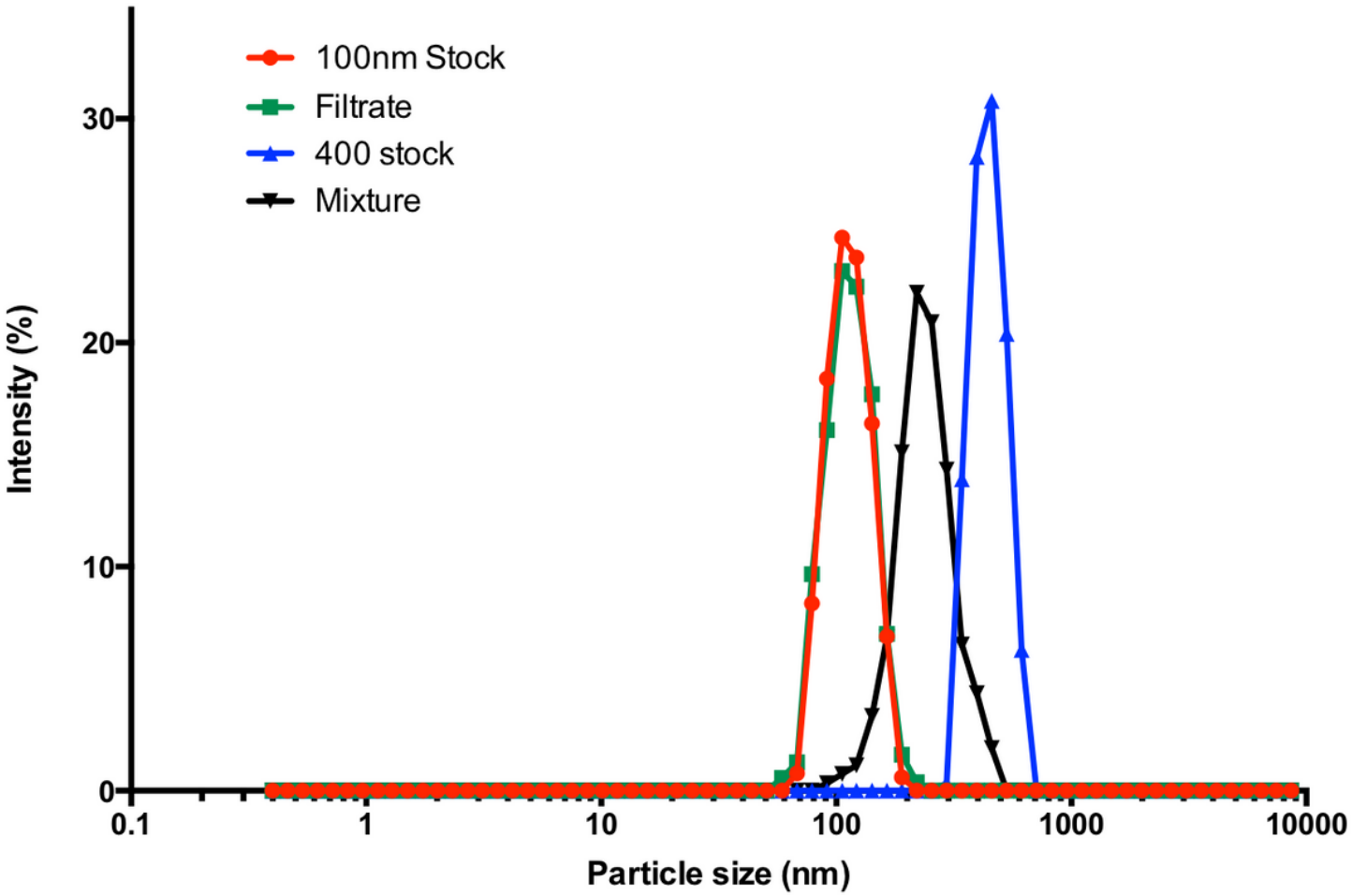


**Figure 7**

Fractionation of 100nm polystyrene NP from polydisperse mixture solution by using ultrasonic-assisted microfluidic particle sorting. Dynamic light scattering (DLS) spectra were obtained from the filtrate (Green) and a mixture containing 1:1 polydisperse 100nm and 400 nm particles (Black). Light scattering spectra of a stock solution of 100nm and 400 nm were obtained for comparison. (Red and blue respectively) Size distribution of filtrate shows that size of particles collected in the filtrate is close to 100 nm stock solution.

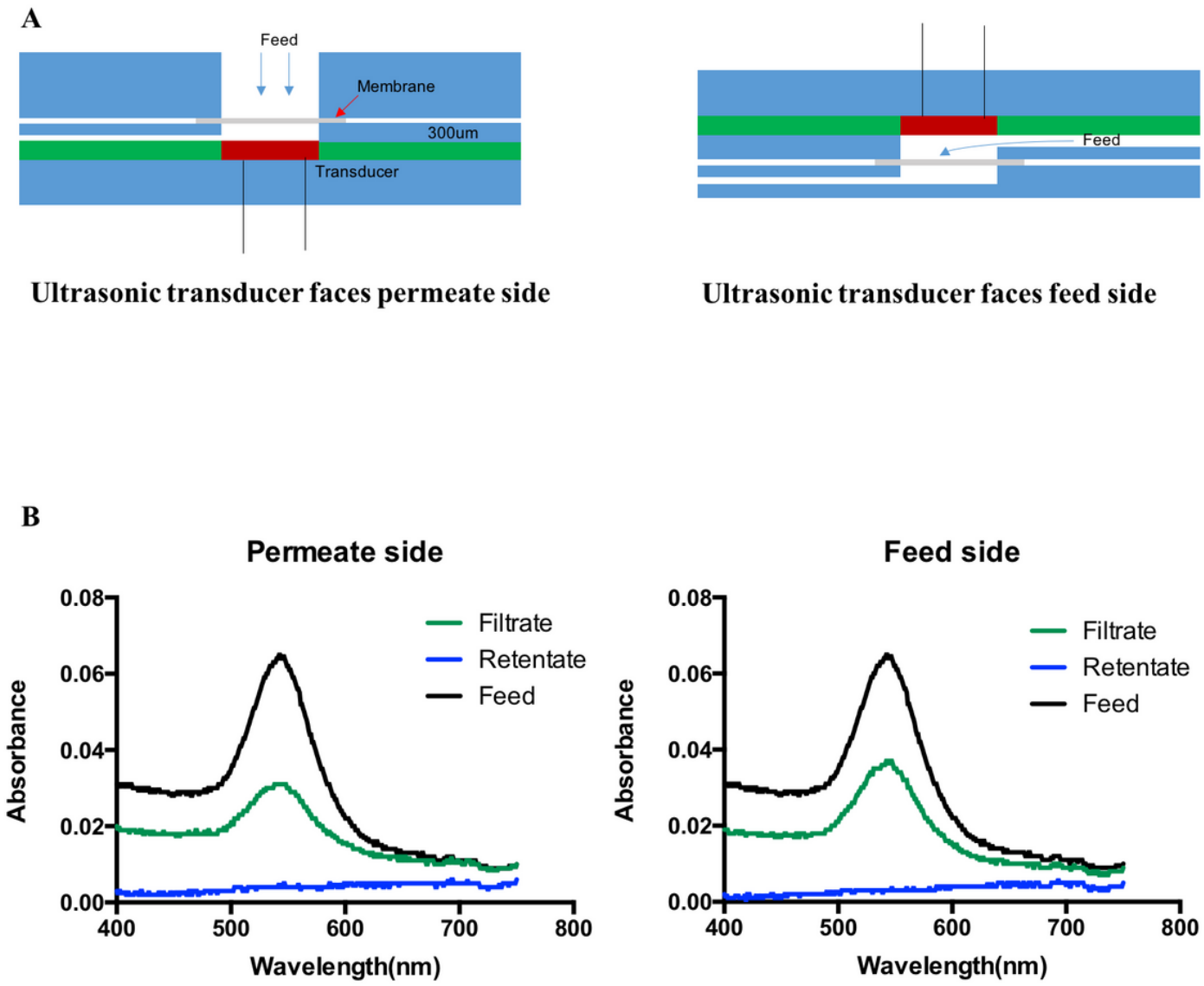


## Figure 8

Effect of the orientation of ultrasonic treatment on recovery rate. Ultrasonic wave with 40 kHz, 40Vp-p output voltage generated by ultrasonic transmitter was focused onto membrane filters either at the permeate side or feed side of the membrane. (A)Layouts of the microfluidic systems for particle filtration for ultrasonic treatment from the membrane filters' permeate side (left) and the feed side (right). The distance between the transducer and membrane remains 300 μm for the experiment. (B) Absorbance spectra of 60 nm Au NP collected in the filtrate solution by ultrasonic treatment from the permeate side (left) and feed side (right) of the membrane filters were compared with the absorbance using an original stock solution of 60 nm Au NP.

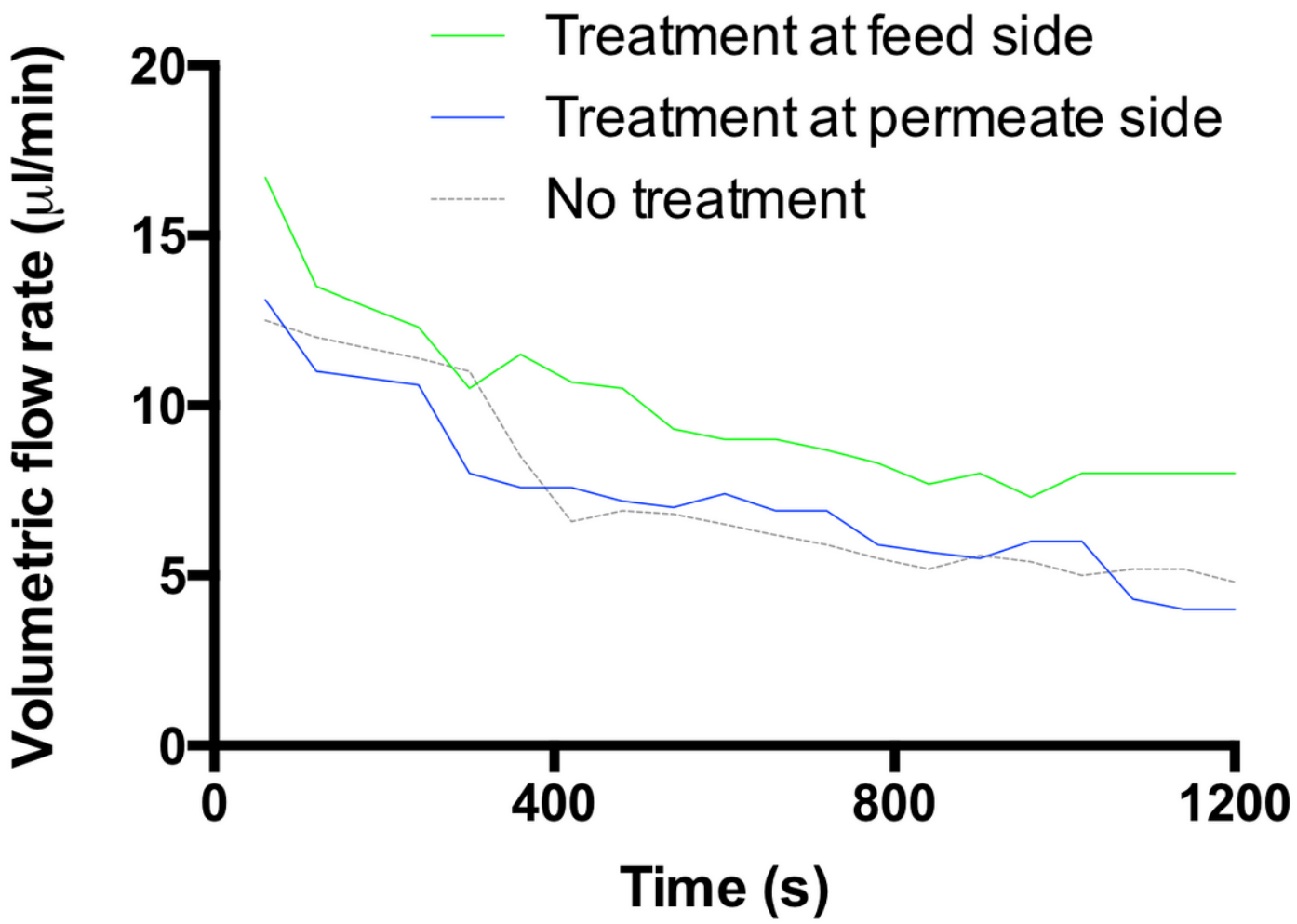


**Figure 9**

Volumetric flow rate of sample filtered using microfluidic particle separation system as a function of filtration time. Samples containing 60 nm Au NP were processed using the microfluidic system with ultrasonic irradiation from the green feed (green) and permeate (blue) or without ultrasonic treatment. As a result, a decrease in flow rate was observed in three cases. However, the highest flow rate was achieved with ultrasonic irradiation from the feed side, and the steady flow rate was observed after 600 sec of the filtration process. For the case of the ultrasound treatment from the permeate side, it showed the same level of fouling as the case of no ultrasound treatment, which indicates that the ultrasonic irradiation is not effective when the ultrasonic waves propagate from the permeate side of the membrane filter